240-GHz Reflectometer-Based Dielectric Sensor With Integrated Transducers in a 130-nm SiGe BiCMOS Technology

Defu Wang, *Member, IEEE*, Mohamed Hussein Eissa, *Member, IEEE*, Klaus Schmalz, Thomas Kämpfe, *Member, IEEE*, and Dietmar Kissinger, *Senior Member, IEEE*

***Abstract*— This article presents a reflectometer-based on-chip dielectric sensor with integrated transducers at 240 GHz. The chip simplifies the measurement of a vector network analyzer (VNA) to sense the incident and reflected waves by using two heterodyne mixer-based receivers with a dielectric sensing element. Radio frequency (RF) and local oscillator (LO) submillimeter waves are generated by two frequency multiplier chains, respectively. Two back-to-back identical differential side-coupled directive couplers are proposed to separate the incident and reflected signals and couple them to mixers. Both transmission line and coplanar stripline transducers are proposed and integrated with reflectometer to investigate the sensitivity of dielectric sensors. The latter leads to a larger power variation of the reflectometer by providing more sufficient operating bands for the magnitude and phase slope of S_{11}. The readout of the transducers upon exposure to liquids is performed by the measurement of their reflected signals using two external excitation sources. The experimental dielectric sensing is demonstrated by using binary methanol–ethanol mixture placed on the proposed on-chip dielectric sensor in the assembled printed circuit board. It enables a maximum 8 dB of the power difference between the incident and reflected channels on the measurement of liquid solvents. Both chips occupy an area of 4.03 mm^2 and consume 560 mW. Along with a wide operational frequency range from 200 to 240 GHz, this simplified one-port-VNA-based on-chip device makes it feasible for the use of handle product and suitable for the submillimeter-wave dielectric spectroscopy applications.**

***Index Terms*— Dielectric sensor, heterodyne, mm-Wave, reflectometer, SiGe, submillimeter-wave, vector network analyzer (VNA).**

I. Introduction

NONINVASIVE and miniaturized dielectric sensors at high frequency are highly required to provide a robust tool to implement accurately detection in biomedical applications, such as estimating the glucose concentration in blood for blood sugar control by allowing the absolute permittivity measurements of human cells with the sensors' scattering parameters in [1]–[4]. High-frequency silicon-based dielectric sensing systems consist of sensing elements and a readout circuit to detect the change in the properties when sensing element upon exposure to the material under test (MUT). Recently reported and demonstrated receiver-based readout circuits are more suitable for providing an ultrawideband dielectric sensing in [5]. Especially, the submillimeter-wave systems draw significant attention due to their high integration level of silicon-based technology with a compact size with their small wavelength. They are based on the vector network analyzer (VNA) concept using either transmission or reflection parameter measurement and both.

Transmission parameter-based dielectric sensors at 1–50 GHz in [6], 120 GHz in [7], and 240 GHz in [8] have been implemented to detect the transmission signal from the change in the characteristics of the sensing element. A comparison of heterodyne and homodyne architecture for it has also been investigated in [9]. Two-port-VNA-based integrated dielectric sensors have been presented with an extended frequency range from 4–32 GHz in [10], 50–100 GHz in [11], and 207–257 GHz in [12] to 300 GHz in [13]. These works show that, while it is possible to build a readout circuit based on transmission and reflection parameters measurement to realize dielectric sensing, there is still more margin left for their simplest form of VNA (reflectometer) featured with only one measurement channel to determine the complex ratio of incident and reflected signals in terms of its relatively low area consumption by a compact form factor for portable low-cost biomedical products.

A detector-based multiprobe and multiport integrated reflectometer is introduced in [14] to enable the phase difference measurement of two electromagnetic waves through amplitudes of several power detectors combined with a multiport junction. A fully integrated multiprobe reflectometer operating at 125 GHz in [15] has been presented to measure the reflected signal for dielectric sensing of liquids in SiGe BiCMOS technology. Similarly, multiport integrated reflectometers have been presented, such as a six-port integrated reflectometer at 3–29 GHz in [16], 30 GHz in [17], and 62 GHz in [18], as well as a five-port integrated reflectometer at 94 GHz in [19].

Manuscript received July 20, 2020; revised October 14, 2020; accepted October 23, 2020. Date of publication December 1, 2020; date of current version January 5, 2021. This work was supported by the Electronic Components and Systems for European Leadership (ECSEL) Joint Undertaking through the Project OCEAN12, Beyond5, and the Deutsche Forschungsgemeinschaft (DFG) Schwerpunktprogramme (SPP) through the ESSENCE project THz-LoC C023CD17. This article was presented at the 2020 International Microwave Conference, Los Angeles, CA, USA, June 20–26, 2020. *(Corresponding author: Defu Wang.)*

Defu Wang and Thomas Kämpfe are with Fraunhofer IPMS, 01099 Dresden, Germany (e-mail: defuwang@ieee.org).

Mohamed Hussein Eissa and Klaus Schmalz are with the IHP–Leibniz-Institut für innovative Mikroelektronik, 15236 Frankfurt (Oder), Germany (e-mail: eissa@ihp-microelectronics.com).

Dietmar Kissinger is with the Institute of Electronic Devices and Circuits, Ulm University, 89081 Ulm, Germany (e-mail: kissinger@ieee.org).

Color versions of one or more figures in this article are available at https://doi.org/10.1109/TMTT.2020.3038382.

Digital Object Identifier 10.1109/TMTT.2020.3038382

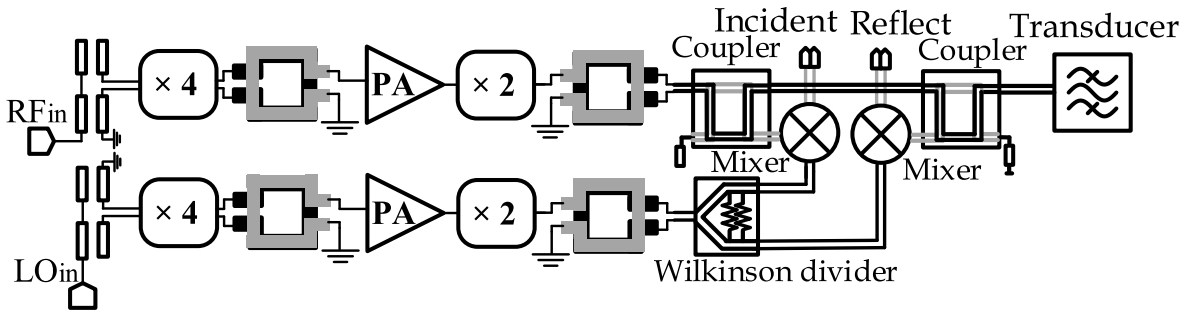

Fig. 1. Block diagram of the 240-GHz heterodyne sensing readout system.

Although they have the advantage of low cost and low power consumption due to its receiver form with a passive linear network and detectors, which also introduces the complexity of calibration and inherent loss of multiport junction and low dynamic range in [20], an alternative reflectometer has overcome this by using an active receiver approach with a high conversion gain. The direct-conversion reflectometers in [21] at 55–77 GHz and in [22] at 60 GHz have been introduced due to its simplicity and friendly integration capabilities. Nevertheless, a mixer-based heterodyne architecture in the design of reflectometer shows superior advantage in terms of dynamic range, which has been shown in [23] at 0.01–26 GHz, [24] at 14–18 GHz, and [25] at 70–110 GHz. By increasing the operational frequency and implementing the on-chip sensing element, it makes the small-fluid-portion and space-restricted possible to have the compact sensing element and microfluidic channel on-chip integration with micrometer-range distance sensing. Due to the different impact of the frequency response of integrated sensing elements to the dielectric sensing introduced in [26], two integrated sensing elements are proposed in this work to integrate with the reflectometer and perform the submillimeter-wave dielectric sensing. They are accomplished with two sensing elements with the open-to-ground termination and a heterodyne-receiver-based reflectometer, including high-frequency signal generation and direction.

In contrast to the original conference paper in [27], this extended version of the manuscript adds one more transducer integrated with the same reflectometer for comparison and details how the circuit blocks work to enable reflection parameter measurement and investigates the phase variation of transducer to readout system as follows:

1) full description of the reflectometer with a special emphasis in transducers: the details of the added second transducer integrated with reflectometer and phase variation at the reflected signal of two transducers and the IF output power of reflected signal with binary methanol : ethanol mixture (concentration in percentage by volume);
2) all detailed circuits of the proposed sensor including directional couplers, two 240-GHz transducers, and two downconversion mixers: the details of design a differential directional coupler; magnitude and phase variation of the transducer with loaded samples; and conversion gain of mixer toward in a large frequency range;
3) measurement setup with the magnified picture of the two chips to test their sensing performance through reflection parameter measurements for both sensors; detailed discussion of the proposed dielectric sensor performance with different sensing elements loaded samples;
4) update of the table for a comparison of reflectometer with different sensing elements.

This article is organized as follows. The reflectometer-based dielectric sensor architecture is presented in Section II. It also gives a detailed discussion of the wideband circuit blocks and their design techniques. Section III demonstrates the presented reflectometer-based sensing system and their simulation results while investigating the transducers. Its performance for dielectric sensing is demonstrated in Section IV, where the materials with different dielectric properties are differentiated using the proposed dielectric sensor.

II. Reflector-Based Sensing Readout Circuit Architecture

A simplified block diagram of the proposed dielectric sensor is shown in Fig. 1. It consists of a transducer as a sensing element and a reflectometer as the readout circuit. Two 240-GHz transducers are chosen for sensing due to that they are based on the modified version of resonator type E (CPS transducer) with wider bandwidth and resonator type A (TL transducer) with higher Q factor in [28] with different dielectric sensitivity followed by their tailored magnitude and phase variation of S_{11}. They were proposed and integrated to investigate the impact of different sensitivities of sensing elements on the system in reflectometer-based dielectric sensors. Although TL transducer creates better sensitivity in magnitude variation at a frequency range from 230 to 240 GHz, the CPS transducer becomes a better candidate by offering a monotonically slope on both magnitude and phase with covering the target frequency range from 200 to 240 GHz. As shown in Fig. 2, the CPS transducer is comprised of two short-ended strips attached together with a shape of a closed polygon. It consists of a wavelength close-ring coplanar stripline (CPS) resonator and an edge-coupled open-ended stub loaded with short-ended stubs demonstrated in [29] and [30]. A partially localized backside etching (LBE) technique is used to remove the loss from the silicon for enhancing the frequency selectivity. Similarly, the TL transducer is proposed with the

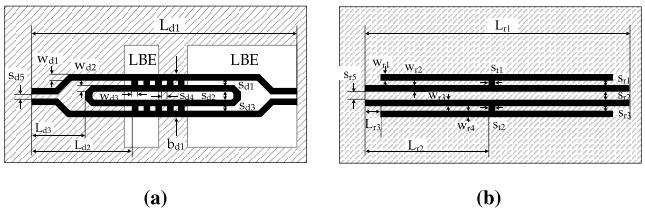

Fig. 2. Structure of (a) CPS transducer and (b) TL transducer.

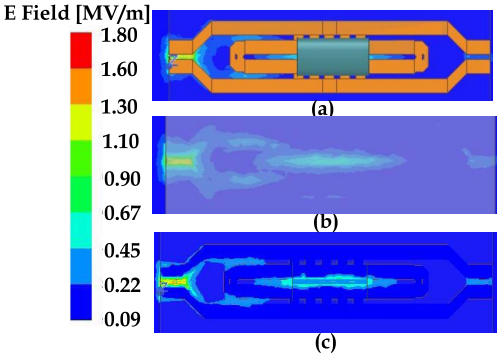

Fig. 3. E-field distribution of the CPS transducer. (a) Top view. (b) Bottom view. (c) Bottom view with the dielectric sample.

resonator type A in [28], which consists of open-ended transmission line (TL) with $W_{r1} = W_{r2} = W_{r3} = W_{r4} = 3.5$ μm width and 635 μm length placed outside the coupled TL designed to operate at center frequency at 240 GHz. The dimension of the TL transducer is selected with a TL length of $L_{r1} = 700$ μm and the line space of $S_{r1} = S_{r3} = 4$ μm and $S_{r2} = 4$ μm. In addition, the width of short-ended stubs is $S_{t1} = S_{t2} = 4$ μm. The chip areas of CPS and TL transducers are 0.1 and 0.02 mm^2, respectively. The larger width of the CPS transducer facilitates realizing LBE and holding the MUTs to have a higher dielectric sensitivity compared with the TL transducer.

Two transducers have been simulated by varying dielectric materials on their top with 3-D planar EM-simulator Ansoft HFSS. The shown amplitudes are calculated for a 1-W reference source power around the resonator transmission without any loaded sample on the sensing surface. The CPS transducer shows a nearly uniform illuminating pattern around the center surface in Fig. 3. It presents that the CPS transducer exposes a strongly localized electric field to the top surface of the chip around the closed short-ended ring resonator. Similarly, a centralized symmetric E-field distribution for the TL transducer shown in Fig. 4 has an $E_{\max}$ of 4.1 MV/m, which is larger than the CPS transducer. A double larger of $E_{\max}$ than the CPS transducer is attributed to more reflected wave on the incident wave, which leads to the larger amplitude and a larger $E_{\max}$. The perturbation of local field distribution in the sensing area of the CPS transducer in Fig. 3(c) and the TL transducer in Fig. 4(c) shows the penetration of the electric field into the liquid. With loading the sample on the sensing surface, the transducer exhibits a symmetry of electric field distribution illuminating pattern on the top surface, which follows the classical resonator arrangement driven by an illumination source from the reflectometer.

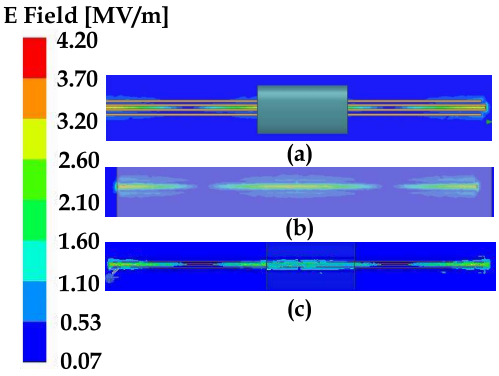

Fig. 4. E-field distribution of the TL transducer. (a) Top view. (b) Bottom view. (c) Bottom view with the dielectric sample.

From the E-field map for transducers in the top and bottom views, good field confinement within the transducer geometry can be recognized.

When exposed to air ($\epsilon_r' = 1$ and $\epsilon_r'' = 0$), the transducer ideally behaviored as bandpass-filter frequency response. When exposed to the MUT, ($\epsilon_r(\omega) = \epsilon_r'(\omega) - j\epsilon_r''(\omega)$), S_{11} of transducer changes, as shown in Fig. 5. The frequency shift of S_{11} changes with the real part of the permittivity independent of the material's loss. The change in material's loss or imaginary part of the permittivity results in a change in the magnitude of S_{11}, independent of the material's frequency shift [31]. Therefore, the change in the frequency-dependent capacitance is translated into a change in the phase shift of the microwave signal passing through the transducer, which is used to estimate ϵ_r' of the MUT. The change in electromagnetic disturbance according to the permittivity $\epsilon = f(\epsilon', \tan\delta)$ of MUTs is translated into a change in reflection coefficient $S_{11}(\omega(\epsilon'), \tan\delta)$ of the transducer, which is then translated into a change in the reflected signal that is coupled into the receiver through the nearby directive coupler for detecting the reflected signal. Therefore, the change at its coupled signal is then read out at the reflection receiver channel. Based on this, a cylinder sample with a diameter of 40 μm and a 150-μm length is employed and exposed on the edge of the CPS and TL transducers as the dielectric MUT in the simulation of the change in S_{11} for permittivity detection. The magnitude and phase variations of S_{11} with different $\tan\delta$'s at a fixed value of $\epsilon' = 5.5$ are simulated in Fig. 5. It can be observed that the magnitude variation of S_{11} is mainly dominated by the change in $\tan\delta$. A variation of ϵ' at a fixed value of $\tan\delta$ does not introduce any change in magnitude but results in a phase variation of S_{11}. Meanwhile, there is a change in $\tan\delta$ without introducing a neglectable frequency shift of S_{11}. Compared with S_{11} of two transducers, the CPS transducer shows a worse return loss, which results in a less deviation of the center frequency and in the low quality of the match with a change in the dielectric. Due to the resonator type E in [28], it can keep better sensitivity by maintaining the wideband peaks in the reflection channel of the reflectometer.

The 240-GHz reflectometer-based readout circuit with integrated CPS transducer and TL transducer is proposed, respectively. The schematic is shown in Fig. 6. It includes a

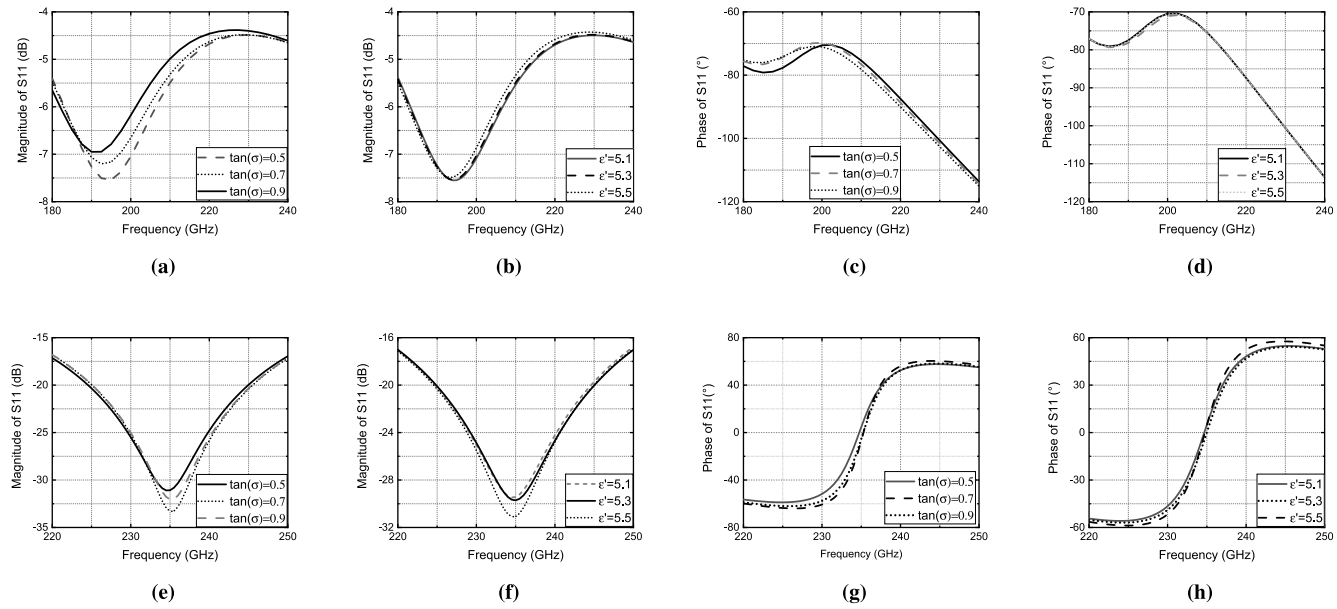

Fig. 5. Simulated magnitude and phase of the reflection coefficient of (a)–(d) CPS transducer and (e)–(h) TL transducer at a fixed $\epsilon' = 5.5$ or $\tan(\sigma) = 0.5$.

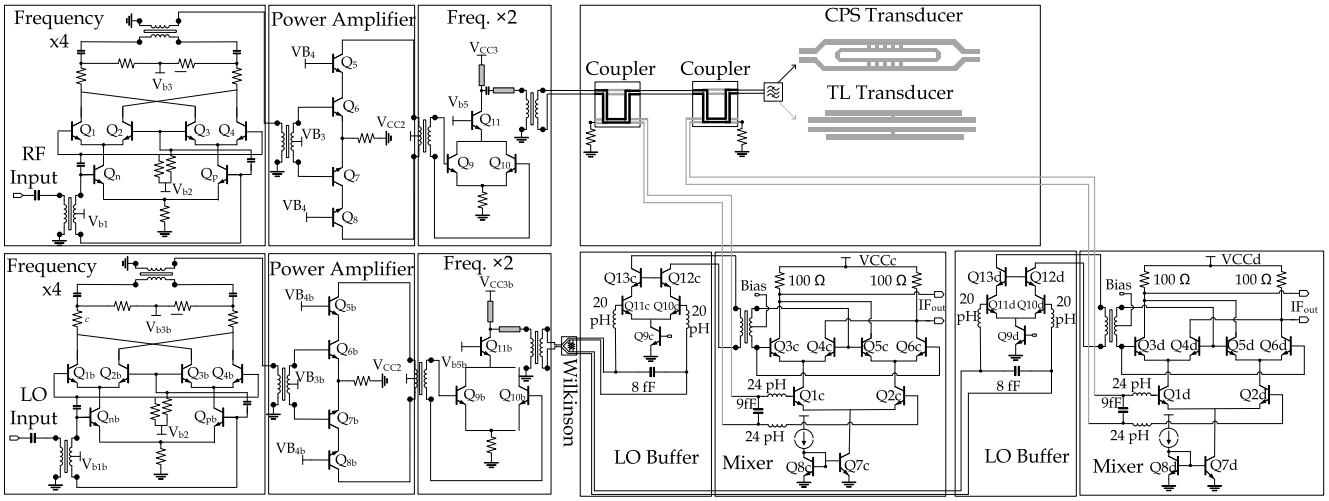

Fig. 6. Schematic of the 240-GHz reflectometer with integrated transducers.

240-GHz radio frequency (RF) and local oscillator (LO) chains for signal generation, directional couplers for signal separation, the CPS or TL transducer as sensing element, and downconversion mixers for readout. The high-frequency signal generation component is realized by 120-GHz frequency quadrupler sourced with a 30-GHz excitation, a 120-GHz power amplifier, and a 120-GHz frequency doubler. The detailed implemented circuits are shown in Fig. 6. It consists of the Gilbert-cell-based architecture for a 120-GHz frequency quadrupler and differential pair with a common-collector architecture to connect the cascode transistor for a 240-GHz frequency doubler. To enhance the signal, a one-stage cascode differential amplifier is used to drive the 240-GHz frequency doubler. The simulated RF/LO chain delivers an output power of 0 dBm at a frequency around 240 GHz. Such an RF signal is connected by a directive coupler to take the RF signal as an incident/reference signal.

As described earlier, each of the reflectometer chips features a proposed wideband differential directional coupler employing in back-to-back by two to maximally isolate the incident and reflected channels and allow to independently define the amount of coupled energy to the incident and reflected channels by using couplers with different transmission and coupling properties. The directional coupler is realized as a side-coupled topology. An illustration of the coupler structure along with the used top metal layer stack is shown in Fig. 7. The differential ground-shielding microstrip lines are used to realize the coupling lines, where the distance between the coupled lines is 3 μm and the metal width of the signal–gap–signal of 9–3–9 μm was adjusted to achieve the required line characteristic impedance and coupling factor. The simulated characterization of this directional coupler in Fig. 8 shows that it has an insertion loss S_{21} of 2.5 dB, a coupled power S_{31} of 7 dB, an isolation S_{41} of 18 dB at an ultrawide bandwidth from 150 to 300 GHz.

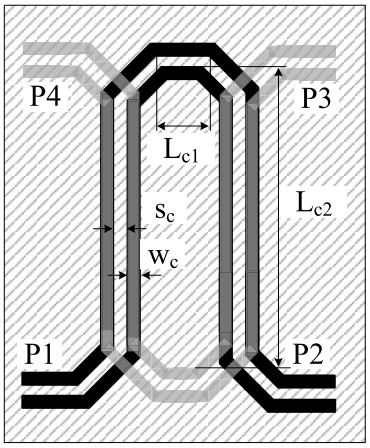

Fig. 7. Structure of the differential directional coupler.

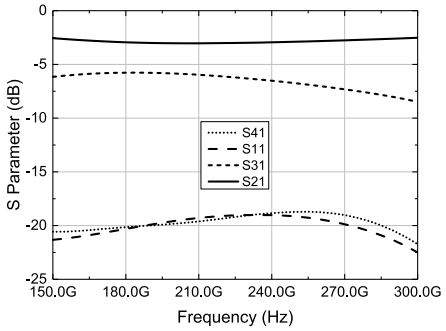

Fig. 8. Simulated scatter parameters of the 240-GHz differential directional coupler.

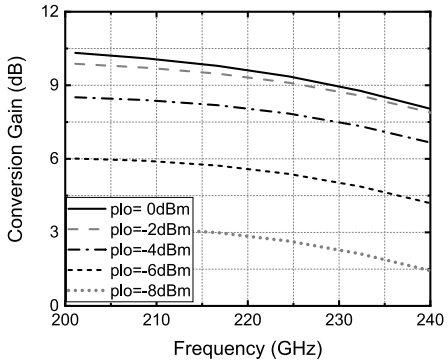

Fig. 9. Simulated conversion gain of mixer versus RF frequency with different LO powers at an RF power of −60 dBm.

In order to sense the incident and reflected signal, 240-GHz receiver consists of a downconversion mixer, and an LO buffer has been demonstrated in Fig. 8 It is based on the Gilbert cell topology. A simulated maximum conversion gain of 10 dB is obtained with a frequency range of 200–240 GHz at a varying of LO powers from −8 to 0 dBm in Fig. 9. It shows that a large LO power is highly required for maintaining a high conversion gain of the mixer. Therefore, a cascode differential amplifier topology of LO buffer is employed to enhance the LO power of mixer with matching at 100-Ω output impedance of the Wilkinson power divider. Fig. 10 shows that an LO power of less than 0 dBm relaxes the 1-dB compression point of mixer although it provides a lower conversion gain.

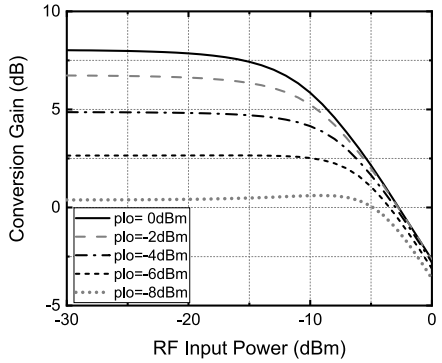

Fig. 10. Simulated conversion gain of mixer versus RF input power with different LO powers at 240 GHz.

The proposed mixers are used to create a reflectometer that is provided by an RF and LO power of 0 dBm at 30 GHz. By connecting the reflectometer to the CPS and TL transducers, it has a comparison of simulated RF powers at the RF port of mixers shown in Fig. 11(a). Due to the larger dissipated power from CPS transducer, the RF power fed to RF port of mixer at the reflected channel is obviously lower than the one with TL transducer although there is a neglectable difference at the incident channel due to the good isolation of directional couplers. An extra phase added at the end terminal of the transducer with an ideal phase shift from 0° to 90° is employed in the simulation to investigate the phase sensitivity of sensing elements in the system. Fig. 11(b) shows the introduced reflection power variations in the reflectometer at 240 GHz for both transducers.

It shows that the designed CPS transducer leads to a larger power variation at the reflected channel of reflectometer around 240 GHz with the same phase shift as the TL transducer. This difference will be transferred into the difference of the IF output powers at the reflected channel of the reflectometer in the fabrication chips.

The proposed chips have been fabricated in 130-nm IHP SiGe technology, which offers 5-thin and 2-thick aluminum metal layers and has transistors with a cutoff frequency of $f_T = 300$ GHz and $f_{\max} = 500$ GHz, respectively. They occupy the identical silicon area of 3.1×1.3 mm^2 and have a total power consumption of 560 mW. Die micrographs are depicted in Fig. 12. They have been wired-bonded to a printed circuit board (PCB) in Fig. 13 for detecting the complex permittivity of organic liquids, such as isopropanol and different ethanol/methanol mixtures.

III. Dielectric Sensor Experimental Results

Both chips were measured on an assembled board first with air over the transducer and then wire-bonded as a die-on-board with very short wires to keep its parasitic effects as less as possible for dielectric measurements. The dc signals were supplied directly and occupied two pins from 20-pitch dc probe on the top of die, while the synchronized external excitation sources were fed to RF and LO multiplier chains by GSG coaxial probes from two R&S signal generators with a varying of frequencies and power levels. The output power at the intermediate frequency was measured on a

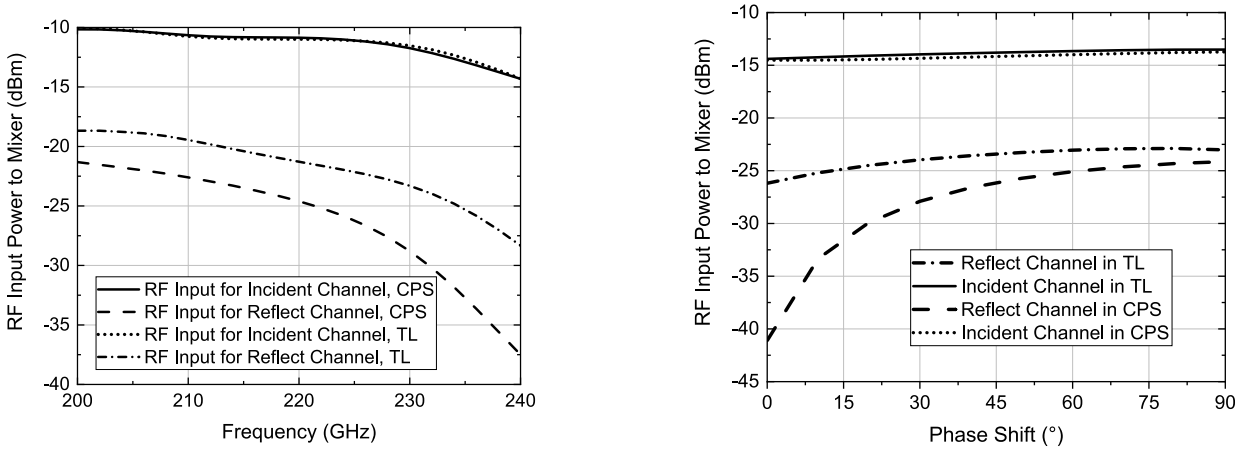

Fig. 11. Simulated RF input power level to RF port of mixer versus (a) frequency and (b) phase shift for receivers at the incident channel and the reflected channel.

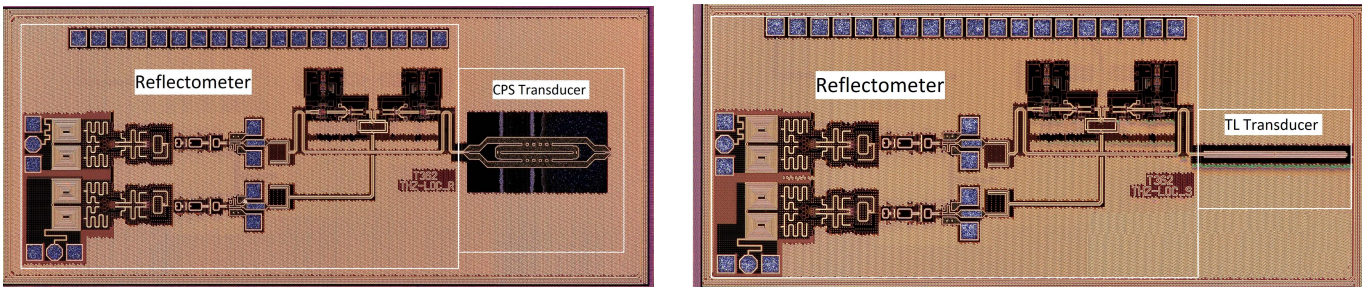

Fig. 12. Die microphotograph of the fabricated 240-GHz reflectometer-based dielectric sensor with integrated (a) CPS transducer and (b) TL transducer.

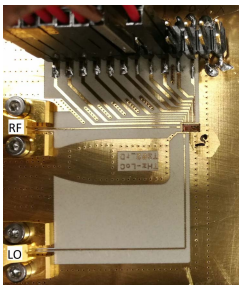

Fig. 13. Photo of the dielectric sensor wire-bonded on PCB.

spectrum analyzer. The assembled boards were also measured with isopropanol and a mixture of methanol and ethanol to have different dielectric sensings. The temperature was held at room temperature when placing liquid solvents over the transducer. As the change in liquid introduces the change in permittivity on both real and imaginary parts, the change in the IF power at the reflected port is mainly due to the change in both. The measurement results of the CPS transducer are shown in Fig. 14. It characterizes using isopropanol and three mixtures of methanol–ethanol with a range from 25% methanol to 75% ethanol by a concentration step of 25%. The measured output power at the incident channel varies between 0.05 to 0.8 dB, as shown in Fig. 14(a), while the measured output power at reflected channel varies between 0.05 and 2.1 dB, as shown in Fig. 14(b). A dielectric with a mixture ratio of 25% methanol to 75% ethanol introduces a nonconstant variation step of output power at both the incident and reflected channels. This effect is mainly attributed to the nonlinear behavior of permittivity when the solutions of different dielectric properties are mixed. A similar effect can also be observed in the results presented in [11] and [15]. Compared with the two figures, it shows that the reflected signal has been separated from the incident signal, which results in more than 8-dB output difference between the incident and reflected channels. Furthermore, the output variation range in the reflected channel has 2 dB larger than the incident channel at a frequency range of 202–224 GHz. In addition, it is more sensitive to the dielectric compared with the incident channel.

Furthermore, a comparison of the measured IF output power of reflectometer with integrated CPS and TL transucer exposed in air are shown in Figs. 15 and 16, and in water is shown in Fig. 17. A large input power dynamic range is obtained with the value from −2 to 7 dBm at 30 GHz in Fig. 15.

The maximum output power of −8 dBm is achieved at the incident channel of sensor with CPS transducer thanking for the large conversion gain of receiver under such operating conditions.

A comparison to prior reflectometer-based dielectric sensor is shown in Table I. This work uses the heterodyne mixers with a differential side-coupling directional coupler to realize a

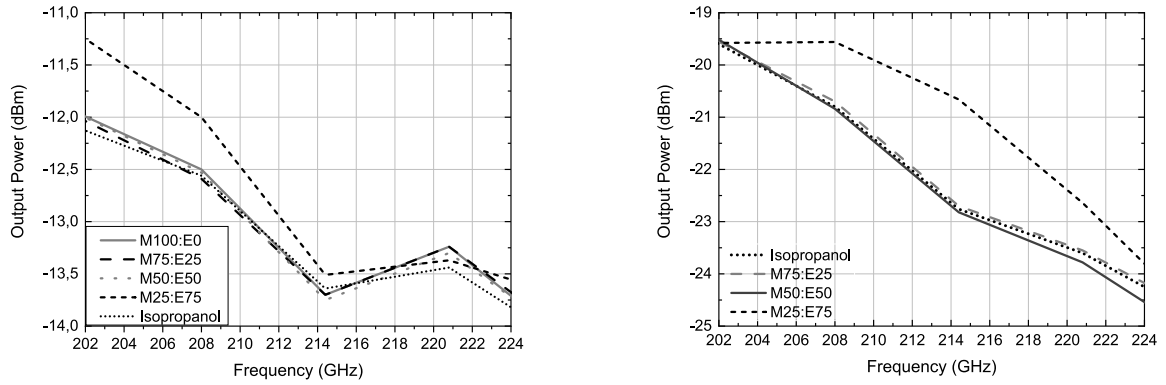

Fig. 14. Measured sensor output powers versus RF input frequency with different mixture ratios of methanol to ethanol over CPS transducer at (a) incident channel and (b) reflected channel.

TABLE I
PERFORMANCE SUMMARY AND COMPARISON WITH STATE-OF-THE-ART mm-WAVE REFLECTOMETER-BASED DIELECTRIC SENSOR

	[15]	[18]	[19]	[21]	[22]	[24]	[25]	This Work
Available Freq. Range	125 GHz	62 GHz	94 GHz	55-77 GHz	60 GHz	14-18 GHz	70-110 GHz	200-240 GHz
Technology	250 nm BiCMOS	250 nm BiCMOS	130 nm BiCMOS	350 nm BiCMOS	130 nm BiCMOS	350 nm BiCMOS	120 nm BiCMOS	130 nm BiCMOS
Architecture	Multi-probe	Six-port	Five-port	Direct-conver.	Direct-conver.	Heterodyne	Heterodyne	Heterodyne
Mixer/Detector numbers	4 dectectors	4 dectectors	3 dectectors	IQ mixer	IQ mixer	2 mixers	2 mixers	2 mixers
Sensing Element Integration Level	On Chip	On Chip	Off Chip	Off Chip	Off Chip	On Chip	N/A	On Chip
Sensing Element	Shorted CPW	Dummy Reson.	Shorted CPW	N/A	Opened TL	Opened coaxial	N/A	Opened CPW/TL
Coupling Structures	1 TL side coupl.	2 TL side coupl.	1 TL connected	N/A	2 diff. side coupl.	2 side coupl.	N/A	2 diff. side coupl.
Input Excitation	Self-sustained	Self-sustained	Self-sustained	Self-sustained	Self-sustained	Ex. 60G	Ex.8.75-13.75G	Ex.25-30G
Sample Materials	Mixtures of Ethanol and Methanol	Voltage-tuned voltage w/o sample	Length-tuned open load w/o sample	N/A	Mixtures of Ethanol and Methanol	Mixtures of Ethanol and Methanol	N/A	DI-water, Mixtures of Ethanol, Methanol
Intermediate Frequency	Mag.of Detector	Mag.of Detector	Mag.of Detector	200 MHz	DC	1 GHz, 20 KHz	1 MHz	800 MHz
Power	247.5 mW	282 mW	6.28 mW	1 W	64.35 mW	132mW	440 mW	560 mW
Chip Area	1.4 mm^2	0.9 mm^2	0.74 mm^2	1.22 mm^2	2.1 mm^2	N/A	5.86 mm^2	4.03 mm^2

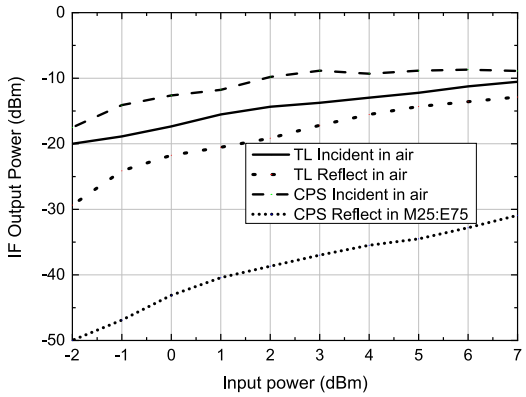

Fig. 15. Measured output powers of incident versus RF input power with air over CPS and TL transducers.

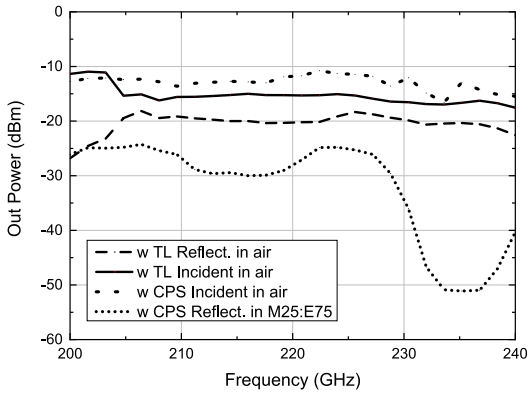

Fig. 16. Measured output powers of the incident and reflected channels versus RF input frequency with air and a mixture ratio of methanol to ethanol with 75% over CPS and TL transducers, respectively.

reflectometer at 240 GHz. Although a large power is consumed comparing to multiport passive receivers, it offers a large external frequency tuning range at an input of 25–30 GHz and facilitates the future integration of microfluidic channel due to their operating at multiplied high frequency, which makes it more suitable for portable biomedical applications. Furthermore, the high integration level of the dielectric sensor with transducers at 240 GHz makes it possible to sense complex permittivity beyond 200 GHz.

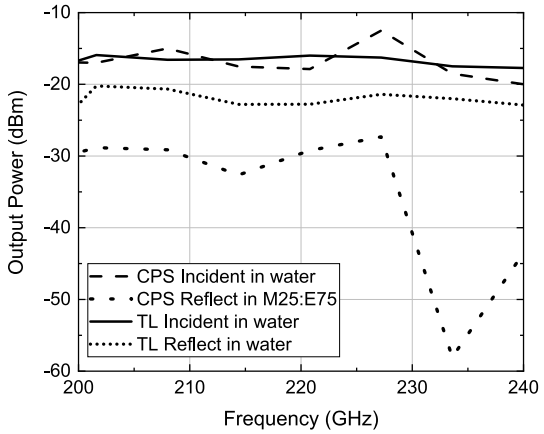

Fig. 17. Measured output powers of the incident and reflected channels versus RF input frequency with water over CPS and TL transducers, respectively.

IV. Conclusion

In this article, a high-frequency miniaturized reflectometer-based dielectric sensor at 240 GHz with integrated transducers has been presented to provide a portable submillimeter-wave lab-on-chip solution. It includes two heterodyne receivers at 240 GHz as the incident and reflected channels to measure the reflection parameter of the 240-GHz transducer. Especially, dielectric sensing occurs when the transducer is loaded with different MUTs. The presented chips feature frequency-multiplier-based stimulus generation with two 30-GHz external sources. They integrate the reflectometer with two 240-GHz transducers in different frequency responses. The experimental measurement has been made using wire-bonded chips on PCB with ethanol in a mixture of methanol. A variation of mixer output power level at an intermediate frequency of 800 MHz demonstrates that the transducer with more sufficient magnitude and phase slope of bandwidth in S_{11} introduces a larger power variation to the reflectometer and leads to the more sensitive dielectric sensor. The proposed reflectometer-based dielectric sensor with the integrated transducer is suitable to use in portable label-free biomedical devices.

Acknowledgment

The authors would like to thank J. Borngraeber, F. Popiela, and J. Witthaus for their support during measurements, board fabrication, and wire bonding.

References

[1] Y. Hayashi, L. Livshits, A. Caduff, and Y. Feldman, "Dielectric spectroscopy study of specific glucose influence on human erythrocyte membranes," *J. Phys. D, Appl. Phys.*, vol. 36, no. 4, pp. 369–374, Feb. 2003.

[2] K. Grenier *et al.*, "Integrated broadband microwave and microfluidic sensor dedicated to bioengineering," *IEEE Trans. Microw. Theory Techn.*, vol. 57, no. 12, pp. 3246–3253, Dec. 2009.

[3] M. Hofmann, G. Fischer, R. Weigel, and D. Kissinger, "Microwave-based noninvasive concentration measurements for biomedical applications," *IEEE Trans. Microw. Theory Techn.*, vol. 61, no. 5, pp. 2195–2204, May 2013.

[4] X. Ma, X. Du, L. Li, H. Li, X. Cheng, and J. C. M. Hwang, "Sensitivity analysis for ultra-wideband 2-port impedance spectroscopy of a live cell," *IEEE J. Electromagn., RF Microw. Med. Biol.*, vol. 4, no. 1, pp. 37–44, Mar. 2020.

[5] K. Entesari, A. A. Helmy, and M. Moslehi-Bajestan, "Integrated systems for biomedical applications: Silicon-based RFMicrowave dielectric spectroscopy and sensing," *IEEE Microw. Mag.*, vol. 18, no. 5, pp. 57–72, Jul. 2017.

[6] J.-C. Chien, M. Anwar, E.-C. Yeh, L. P. Lee, and A. M. Niknejad, "A 1–50 GHz dielectric spectroscopy biosensor with integrated receiver front-end in 65 nm CMOS," in *IEEE MTT-S Int. Microw. Symp. Dig.*, Seattle, WA, USA, Jun. 2013, pp. 1–4.

[7] J. Wessel, K. Schmalz, J. C. Scheytt, and D. Kissinger, "A 120-GHz electrical interferometer for contactless permittivity measurements with direct digital read-out," *IEEE Microw. Wireless Compon. Lett.*, vol. 27, no. 2, pp. 198–200, Feb. 2017.

[8] D. Wang *et al.*, "Integrated 240-GHz dielectric sensor with DC readout circuit in a 130-nm SiGe BiCMOS technology," *IEEE Trans. Microw. Theory Techn.*, vol. 66, no. 9, pp. 4232–4241, Sep. 2018.

[9] D. Wang *et al.*, "Homodyne and heterodyne terahertz dielectric sensors: Prototyping and comparison in BiCMOS technology for lab-on-chip applications," in *Proc. IEEE Int. Microw. Biomed. Conf. (IMBioC)*, Philadelphia, PA, USA, Jun. 2018, pp. 4–6.

[10] J. Nehring *et al.*, "Highly integrated 4–32-GHz two-port vector network analyzers for instrumentation and biomedical applications," *IEEE Trans. Microw. Theory Techn.*, vol. 65, no. 1, pp. 229–244, Jan. 2017.

[11] I. Nasr, J. Nehring, K. Aufinger, G. Fischer, R. Weigel, and D. Kissinger, "Single-and dual-port 50-100-GHz integrated vector network analyzers with on-chip dielectric sensors," *IEEE Trans. Microw. Theory Techn.*, vol. 62, no. 9, pp. 2168–2179, Sep. 2014.

[12] D. Wang *et al.*, "240-GHz four-channel power-tuning heterodyne sensing readout system with reflection and transmission measurements in a 130-nm SiGe BiCMOS technology," *IEEE Trans. Microw. Theory Techn.*, vol. 67, no. 12, pp. 5296–5306, Dec. 2019.

[13] A. J. Alazemi and G. M. Rebeiz, "A 100–300-GHz free-space scalar network analyzer using compact Tx and Rx modules," *IEEE Trans. Microw. Theory Techn.*, vol. 64, no. 11, pp. 4021–4029, Nov. 2016.

[14] A. Koelpin, G. Vinci, B. Laemmle, D. Kissinger, and R. Weigel, "The six-port in modern society," *IEEE Microw. Mag.*, vol. 11, no. 7, pp. 35–43, Dec. 2010.

[15] B. Laemmle, K. Schmalz, J. C. Scheytt, R. Weigel, and D. Kissinger, "A 125-GHz permittivity sensor with read-out circuit in a 250-nm SiGe BiCMOS technology," *IEEE Trans. Microw. Theory Techn.*, vol. 61, no. 5, pp. 2185–2194, May 2013.

[16] F. Trenz, M. Hofmann, R. Weigel, and D. Kissinger, "A broadband 3–29 GHz reflectometer with a frequency compensated multilayer sixport structure," in *Proc. Eur. Microw. Conf. (EuMC)*, Paris, France, Sep. 2015, pp. 323–326.

[17] R. K. Yadav, J. Wessel, M. H. Eissa, F. I. Jamal, M. Kucharski, and D. Kissinger, "A 30 GHz power detector based reflectometer in 130 nm SiGe BiCMOS for dielectric spectroscopy," in *Proc. IEEE Int. Symp. Circuits Syst. (ISCAS)*, Florence, Italy, May 2018, pp. 1–4.

[18] B. Laemmle, K. Schmalz, C. Scheytt, D. Kissinger, and R. Weigel, "A 62 GHz reflectometer for biomedical sensor readout in SiGe BiCMOS technology," in *Proc. IEEE 12th Top. Meeting Silicon Monolithic Integr. Circuits RF Syst.*, Santa Clara, CA, USA, Jan. 2012, pp. 45–48.

[19] J. A. Qayyum, A. A. Nawaz, M. Ko, A. Malignaggi, D. Kissinger, and A. C. Ulusoy, "A 94-GHz five-port reflectometer for measuring complex reflection coefficient using 0.13-μm SiGe HBT detectors," in *Proc. IEEE Top. Conf. Wireless Sens. Sens. Netw. (WiSNet)*, Jan. 2018, pp. 77–79.

[20] D. Kissinger, B. Laemmle, I. Nasr, and R. Weigel, "Millimeter-wave integrated reflectometer architectures for biomedical applications," in *Proc. IEEE Top. Conf. Biomed. Wireless Technol., Netw., Sens. Syst.*, Austin, TX, USA, Jan. 2013, pp. 61–63.

[21] I. Nasr, M. Dudek, R. Weigel, and D. Kissinger, "A 33% tuning range high output power V-band superharmonic coupled quadrature VCO in SiGe technology," in *Proc. IEEE Radio Freq. Integr. Circuits Symp.*, Montreal, QC, Canada, Jun. 2012, pp. 301–304.

[22] R. K. Yadav, M. H. Eissa, J. Wessel, and D. Kissinger, "A 60 GHz mixer-based reflectometer in 130 nm SiGe BiCMOS technology toward dielectric spectroscopy in medical applications," in *Proc. IEEE Int. Microw. Biomed. Conf. (IMBioC)*, Philadelphia, PA, USA, Jun. 2018, pp. 88–90.

[23] H. Chung, Q. Ma, M. Sayginer, and G. M. Rebeiz, "A Packaged 0.01–26-GHz single-chip SiGe reflectometer for two-port vector network analyzers," *IEEE Trans. Microw. Theory Techn.*, vol. 68, no. 5, pp. 1794–1808, May 2020.

[24] J. Nehring, M. Schuetz, R. Weigel, and D. Kissinger, "A microwave permittivity sensing system based on a hybrid heterodyne reflectometer circuit," in *Proc. 44th Eur. Microw. Conf.*, Rome, Italy, Oct. 2014, pp. 159–162.

[25] B.-H. Ku, H. Chung, and G. M. Rebeiz, "A 70–110 GHz single-chip SiGe reflectometer with integrated local oscillator quadrupler," in *IEEE MTT-S Int. Microw. Symp. Dig.*, Honolulu, HI, USA, Jun. 2017, pp. 980–982.
[26] F. I. Jamal *et al.*, "Low-power miniature *K*-band sensors for dielectric characterization of biomaterials," *IEEE Trans. Microw. Theory Techn.*, vol. 65, no. 3, pp. 1012–1023, Mar. 2017.
[27] D. Wang, M. H. Eissa, K. Schmalz, T. Kampfe, and D. Kissinger, "240-GHz reflectometer with integrated transducer for dielectric spectroscopy in a 130-nm SiGe BiCMOS technology," in *IEEE MTT-S Int. Microw. Symp. Dig.*, Los Angeles, CA, USA, Aug. 2020, pp. 1–3.
[28] Y.-H. Suh and K. Chang, "Coplanar stripline resonators modeling and applications to filters," *IEEE Trans. Microw. Theory Techn.*, vol. 50, no. 5, pp. 1289–1296, May 2002.
[29] K. Schmalz *et al.*, "A 120 GHz dielectric sensor in SiGe BiCMOS," *IEEE Microw. Wireless Compon. Lett.*, vol. 23, no. 1, pp. 46–48, Jan. 2013.
[30] D. Wang, K. Schmalz, J. Borngräber, and D. Kissinger, "On-chip scalable resonator-based transducers for terahertz dielectric sensing in SiGe BiCMOS technology," in *Proc. 30th Asia Pacific Microw. Conf.*, Kyoto, Japan, Nov. 2018, pp. 240–242.
[31] A. A. Helmy and K. Entesari, "A 1–8-GHz miniaturized spectroscopy system for permittivity detection and mixture characterization of organic chemicals," *IEEE Trans. Microw. Theory Techn.*, vol. 60, no. 12, pp. 4157–4170, Dec. 2012.

Defu Wang (Member, IEEE) received the M.Sc. degree in electromagnetic fields and microwave techniques from the Harbin Institute of Technology, Harbin, China, in 2010, and the Dr.Ing. degree in electrical engineering from RWTH Aachen University, Aachen, Germany, in 2019.

From 2010 to 2015, he was a Research Assistant with the Chair of High Frequency Electronics, RWTH Aachen University. In 2015, he joined the Circuit Design Department, IHP Microelectronics, Frankfurt (Oder), Germany, where he worked on the development of wideband submillimeter-wave systems for sensing and communications. Since 2019, he has been with the Center Nanoelectronic Technologies (CNT), Fraunhofer-IPMS, Dresden, Germany, where he is involved in the development of millimeter-wave circuits for communications and sensing, and nonvolatile memory IP products. His research interests include wideband RF, millimeter- and submillimeter-wave integrated circuits in silicon technologies for communication, radar, and dielectric spectroscopy, as well as the intelligent integrated circuits for neuromorphic computing.

Dr. Wang was a recipient of the Silver Award of the IEEE Conference on Ph.D. Research in Microelectronics & Electronics in 2012.

Mohamed Hussein Eissa (Member, IEEE) received the B.Sc. degree from Ain Shams University, Cairo, Egypt, in 2009, the M.Sc. degree from The American University in Cairo, New Cairo, Egypt, in 2014, and the Ph.D. degree from Technical University Berlin, Berlin, Germany, in 2019.

He worked for two years with Silicon Vision LLC, Cairo, involved in the design of ASICs for Bluetooth communication standards. From 2011 to 2014, he was with Hittite Microwave, Cairo, working on the design of transceivers for point-to-point communication. Since October 2014, he has been a Research Scientist with the Circuit Design Department, IHP, Frankfurt (Oder), Germany. His research interests include RF and mm-wave circuit designs for communication applications.

Klaus Schmalz received the Ph.D. degree in physics from the Humboldt University of Berlin, Berlin, Germany, in 1978.

He was involved in the field of silicon semiconductor technologies and research for some time and has expertise in the area of thermally induced defects and characterization of Si/SiGe structures. After training in RF circuit design at the University of California at Los Angeles, Los Angeles, CA, USA, from 1998 to 1999, he changed his scientific focus to RF analog circuit design. He is currently with IHP, Frankfurt (Oder), Germany. He has authored or coauthored more than 100 articles. His current research interests include the design of SiGe BiCMOS analog circuits for wireless communication with an emphasis on RF front ends for different standards and mm-wave circuits for sensor applications.

Thomas Kämpfe (Member, IEEE) received the Diploma degree in physics and the Ph.D. degree in applied physics with a focus on ferroelectric devices for memory and microwave applications from TU Dresden, Dresden, Germany, in 2011 and 2016, respectively.

After research visiting scholar positions with the University of Colorado at Boulder, Boulder, CO, USA, and Stanford University, Stanford, CA, USA, he joined the Fraunhofer Society, Munich, Germany, in 2017, where he is currently a group Manager in CMOS Integrated RF & AI. To date, he has authored or coauthored more than 70 peer-reviewed journal articles and conference proceedings. His main research interests include the integration of ferroelectrics for advanced emerging memories and in-memory computing, as well as RF/mmWave devices, circuits, and systems.

Dietmar Kissinger (Senior Member, IEEE) received the Dipl.Ing., Dr.Ing., and Habil. degrees in electrical engineering from the University of Erlangen-Nuremberg, Erlangen, Germany, in 2007, 2011, and 2014, respectively.

From 2007 to 2010, he was with Danube Integrated Circuit Engineering, Linz, Austria, where he was a System and Application Engineer with the Automotive Radar Group. From 2010 to 2014, he was a Lecturer and the Head of the Radio Frequency Integrated Sensors Group, Institute for Electronics Engineering, Erlangen. From 2015 to 2018, he was with Technische Universität Berlin, Berlin, Germany, and the Head of the Circuit Design Department, IHP, Frankfurt (Oder), Germany. Since 2019, he has been a Full Professor of high-frequency circuit design with Ulm University, Ulm, Germany, where he has been the Head of the Institute of Electronic Devices and Circuits. He has authored or coauthored over 300 technical articles. He holds several patents. His current research interests include silicon high-frequency and high-speed integrated circuits and systems for communication and automotive, industrial, security, and biomedical sensing applications.

Dr. Kissinger has served as a member of the 2013 and 2017 European Microwave Week (EuMW) Organizing Committee and the 2018 IEEE MTT-S International Microwave Symposium (IMS) Steering Committee and the Executive Committee Chair of the Radio and Wireless Week (RWW). He is also an elected member of the IEEE MTT-S Administrative Committee. He is also a member of the European Microwave Association (EuMA), the German Information Technology Society (ITG), and the Society of Microelectronics, Microsystems and Precision Engineering (VDE/VDI GMM). He also serves as a member of the Technical Program Committee of the International Microwave Symposium (IMS), the European Solid-State Circuits Conference (ESSCIRC), and the Technical Program Committee of the European Microwave Week (EuMW) and the TPC Chair of the 2021 German Microwave Conference (GeMiC). He received the 2017 IEEE MTT-S Outstanding Young Engineer Award, the 2017 VDE/VDI GMM-Prize, and the 2018 VDE ITG-Prize. He was a co-recipient of more than ten best paper awards. He was a two-time Chair of the IEEE Topical Conference on Wireless Sensors and Sensor Networks (WiSNet) and the IEEE Topical Conference on Biomedical Wireless Technologies, Networks and Sensing Systems (BioWireless). He was the Chair of the IEEE MTT-S Technical Committee on Microwave and Millimeter-Wave Integrated Circuits (MTT-14). He was a nine-time Guest Editor of the *IEEE Microwave Magazine*. He has served as an Associate Editor for the IEEE TRANSACTIONS ON MICROWAVE THEORY AND TECHNIQUES.